12-6-2021

A Modular Strategy for Expanding Electron-Sink Capacity in Noncanonical Cluster Assemblies

Yume Mai
Boise State University

Alexandria K. Balzen
Boise State University

Rebecca K. Torren
Boise State University

Michael P. Callahan
Boise State University

Adam C. Colson
Boise State University

Article

A Modular Strategy for Expanding Electron-Sink Capacity in Noncanonical Cluster Assemblies

Yume Mai, Alexandria K. Balzen, Rebecca K. Torres, Michael P. Callahan, and Adam C. Colson*
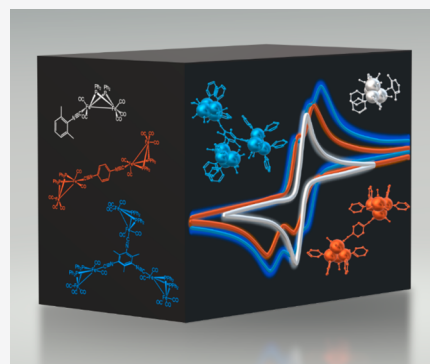
Read Online

ACCESS | Metrics & More | Article Recommendations | Supporting Information

ABSTRACT: A modular synthetic strategy is described whereby organometallic complexes exhibiting considerable electron-sink capacity may be assembled by using only a few simple molecular components. The $Fe_2(PPh_2)_2(CO)_5$ fragment was selected as a common electroactive component and was assembled around aromatic cores bearing one, two, or three isocyanide functional groups, with the resultant complexes possessing electron-sink capacities of two, four, and six electrons, respectively. The latter complex is noteworthy in that its electron-sink capacity was found to rival that of large multinuclear clusters (e.g., $[Ni_{32}C_6(CO)_{36}]^{6-}$ and $[Ni_{38}Pt_6(CO)_{48}]^{6-}$), which are often considered as benchmarks of electron-sink behavior. Moreover, the modular assembly bearing three $Fe_2(PPh_2)_2(CO)_5$ fragments was observed to undergo reduction to a hexaanionic state over a potential window of about −1.4 to −2.1 V (vs Fc/Fc$^+$), the relatively compressed range being attributed to potential inversions operative during the addition of the second, fourth, and sixth electrons. Such complexes may be designated *noncanonical clusters* because they exhibit redox properties similar to those of large multinuclear clusters yet lack the extensive network of metal−metal bonds and the condensed metallic cores that typify the latter.

INTRODUCTION

Molecular species capable of accumulating multiple charges via sequential redox events are promising candidates as functional materials in emerging technologies such as Faradaic supercapacitors, multistate molecular switches, and charge-based multibit data storage.[1] Compounds exhibiting "electron-sink" properties are broadly distributed across several molecular classes, including the fullerenes, viologens, diimides, polyoxometalates, metallocene-containing dendrimers and polymers, and various coordination and organometallic complexes.[2] Among the latter, multinuclear organometallic clusters are particularly intriguing, as remarkable electron-sink behaviors have been documented in clusters containing 20 or more transition metal nuclei.[3] Benchmark examples of such clusters include the large carbide−carbonyl anion $[Ni_{32}C_6(CO)_{36}]^{6-}$ and the bimetallic $[Ni_{38}Pt_6(CO)_{48}]^{6-}$ anion, both of which may accommodate up to five electrons per discrete molecular unit.[4]
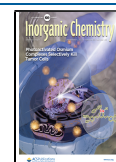
Despite these distinctive electronic properties, the maturation of large organometallic clusters as viable functional materials has been limited by the complexity of existing synthetic methods that rely on thermal, photochemical, or redox condensation reactions to expand total cluster nuclearity, often resulting in broad or unpredictable product distributions.[5] Consequently, the intentional design of high-capacity electron-sink clusters remains an enduring challenge in metal cluster chemistry.

For more than 50 years, clusters have been canonically defined as discrete molecular species containing three or more metal atoms mutually connected by metal−metal bonds, a category into which the previously mentioned $[Ni_{32}C_6(CO)_{36}]^{6-}$ and $[Ni_{38}Pt_6(CO)_{48}]^{6-}$ complexes clearly fall.[6] More recently, reports have emerged of organometallic complexes whose electron-sink properties bear similarities to those of large canonical clusters but do not conform to the classical definition. For example, Wang and Sun have reported that the reaction of $Fe_3(CO)_{12}$ with 1,2,4,5-benzenetetrathiol or benzenehexathiol produces diiron dithiolate complexes in which two or three $Fe_2S_2(CO)_6$ subunits are linked by a common aromatic bridge.[7] Under cathodic conditions, the resultant complexes can accommodate either four or six electrons to yield anions with charges of 4− and 6−, respectively. Nuckolls et al. have also described the electrochemical properties of "superatom" complexes prepared by tethering multinuclear $Co_6Se_8(P(C_2H_5)_3)_5$ subunits together by using an aryl diisocyanide linker.[8] In contrast with the preceding examples, the tethered $Co_6Se_8(P(C_2H_5)_3)_5$ complexes undergo a series of oxidation steps under anodic conditions to yield highly charged cations. These cations may also be regarded as possessing significant electron-sink

capacity, as the electron "holes" produced during oxidation may be repopulated with electrons to restore the neutral parent complexes under cathodic conditions.

The organometallic complexes described above may be conveniently termed *noncanonical clusters* because they exhibit redox properties comparable to those of large multinuclear clusters yet lack the extensive network of metal−metal bonds and the condensed metallic cores characteristic of the latter. As the cited examples demonstrate, the noncanonical approach to cluster synthesis lends itself to the intentional design of molecular materials with predictable molecular architectures and redox properties, making noncanonical clusters convenient models for exploring electron-sink phenomena and potential applications associated therewith.

The purpose of this study is to establish a modular synthetic strategy whereby noncanonical cluster complexes with significant electron-sink capacity might be assembled by using only a handful of readily accessible molecular components. To this end, the simple $Fe_2(PPh_2)_2(CO)_5$ fragment was used as a common electroactive subunit and was tethered to aromatic isocyanides bearing one, two, or three functional groups. The electron-sink capacities of the resultant complexes were progressively expanded from two, to four, to six electrons, respectively, the latter exceeding the electron-sink capacity of canonical benchmark clusters (e.g., $[Ni_{32}C_6(CO)_{36}]^{6-}$ and $[Ni_{38}Pt_6(CO)_{48}]^{6-}$).

■ RESULTS AND DISCUSSION

The modular synthetic strategy reported herein comprised three steps, the first of which was to identity a well-characterized compound capable of accommodating multiple electrons under cathodic conditions. We were drawn to $Fe_2(PPh_2)_2(CO)_6$ (1) (Figure 1) as a parent electroactive complex based on its structural simplicity and convenient, scalable synthesis.[9] More importantly, it has been proposed that $Fe_2(PPh_2)_2(CO)_6$ undergoes a reversible two-electron reduction as a consequence of *redox potential inversion*, a phenomenon that warrants a brief discussion.[9a,10] When two electrons are transferred to a molecular species in the *absence* of a potential inversion, the second electron is transferred with greater difficulty than the first, and the potential required to effect the second electron transfer becomes more negative. When potential inversion is operative, the formal potential corresponding to the addition of the second electron becomes more *positive* than that of the first, often by several tenths of a volt.[11] In such cases, the transfer of the second electron cannot be detected independent of the first by using conventional voltammetric methods; rather, the voltammetric response gives the impression of a simultaneous two-electron transfer. Potential inversion is almost universally associated with a significant molecular organization, and $Fe_2(PPh_2)_2(CO)_6$ appears to be no exception: X-ray diffraction studies of 1^{2-} reveal that the "butterfly"-like structure of the neutral complex undergoes a dramatic reorganization during reduction in which the Fe_2P_2 core adopts a flattened configuration.[12]

The second step of our synthetic strategy emphasized the identification of organic "tethers" suitable for binding multiple subunits of 1, thereby expanding the electron-sink capacity of the resulting covalent assembly. As isolobal analogues of carbon monoxide, organic isocyanides are well-suited for binding low-valent transition metals, including the constituent Fe atoms of our preferred electroactive subunit.[14] Ligands bearing multiple isocyanide moieties—some quite exotic—
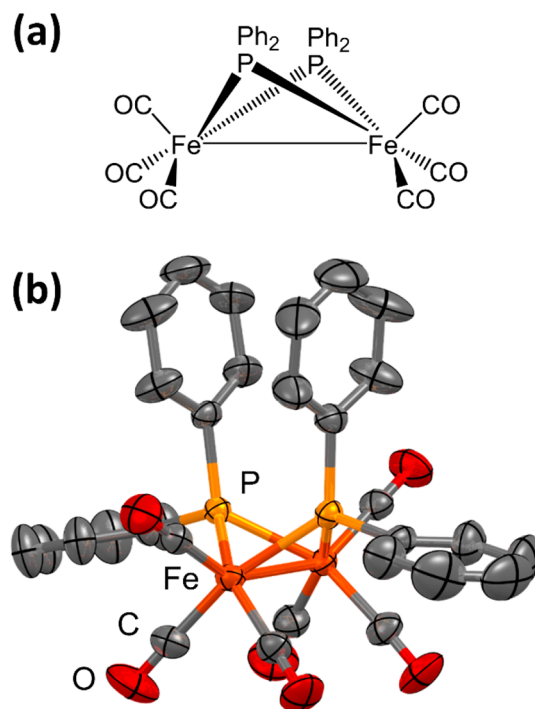

Figure 1. (a) Schematic and (b) molecular structures of $Fe_2(PPh_2)_2(CO)_6$ (1). Color scheme: iron, orange; phosphorus, yellow; carbon, gray; oxygen, red. Hydrogen atoms are excluded; all other thermal ellipsoids are rendered at the 50% probability level (reproduced from CCDC 978092).[13]

have previously been used to prepare extended coordination polymers, supramolecular assemblies, molecular wires, and three-dimensional framework materials.[15] For the purposes of this study, electroactive $Fe_2(PPh_2)_2(CO)_5$ fragments were appended to three very simple aromatic ligands bearing *n* isocyanide moieties: 2,6-dimethylphenyl isocyanide (2a, *n* = 1), 1,4-phenylene diisocyanide (2b, *n* = 2), and 2,4,6-triisocyanomesitylene (2c, *n* = 3). Isocyanides 2a and 2b may be purchased commercially or are readily prepared by using inexpensive reagents.[16] Prior to undertaking this study, 2c was previously unknown in the literature; very recently, however, Hsu and co-workers independently reported its synthesis using a method very similar to that used in the present work.[17]

The culminating step of our modular strategy for producing noncanonical cluster complexes was to append $Fe_2(PPh_2)_2(CO)_5$ fragments to monofunctional, difunctional, and trifunctional arylisocyanide ligands, as illustrated in Scheme 1. Adapting the method of Mizuta,[18] an acetonitrile-coordinated derivative of $Fe_2(PPh_2)_2(CO)_6$, 1-NCMe, was prepared through the treatment of 1 with trimethylamine *N*-oxide (TMANO) in acetonitrile and subsequently combined with 2a−2c in the appropriate stoichiometric ratios to produce the corresponding isocyanide-appended complexes bearing one, two, and three $Fe_2(PPh_2)_2(CO)_5$ fragments (3, 4, and 5, respectively).

The molecular structure of 3 was determined by using single-crystal X-ray diffraction methods and is presented in Figure 2a. Selected bond lengths and angles for complexes 1 and 3 are also tabulated in Table 1, a comparison of which reveals that 3 experiences only slight increases in both Fe−Fe bond length (∼0.033 Å) and mean Fe−P−Fe bond angles

Scheme 1. Modular Synthetic Strategy for Producing Redox-Active Assemblies Bearing One (3), Two (4), and Three (5) $Fe_2(PPh_2)_2(CO)_5$ Fragments Appended to Isocyanide Ligands
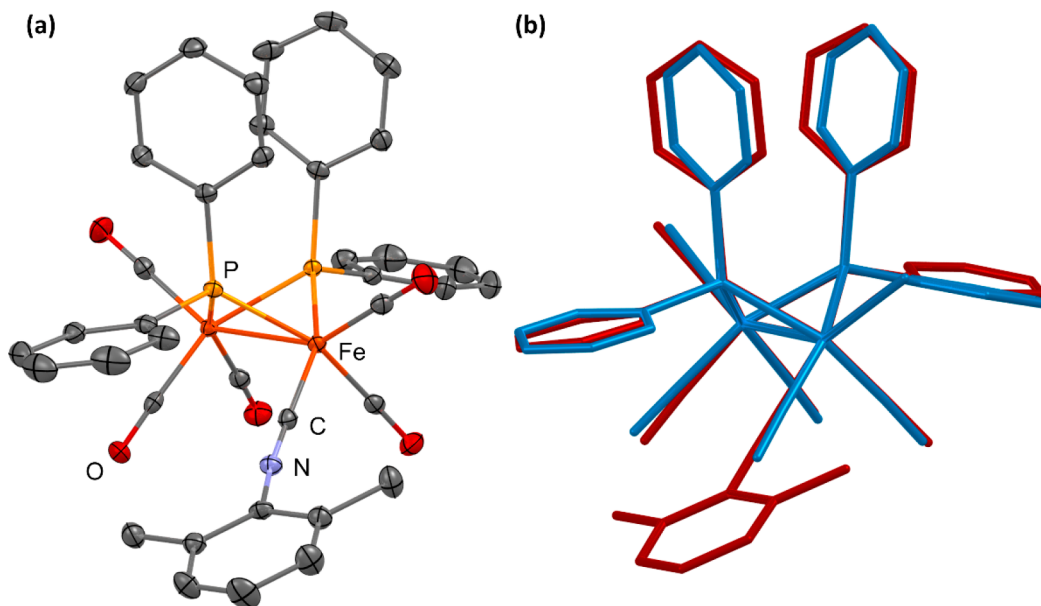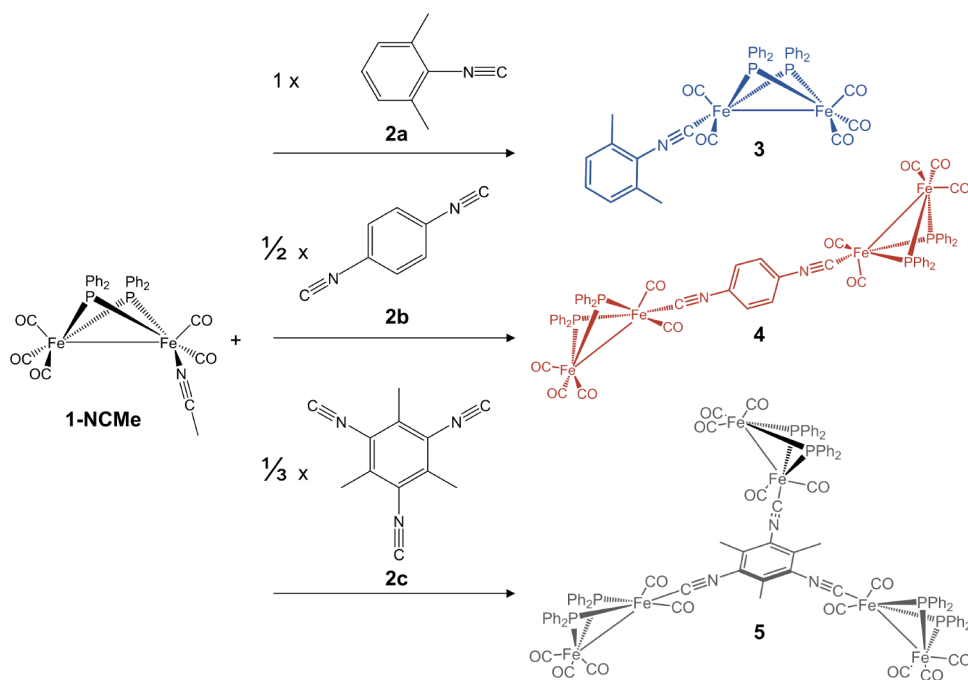

Figure 2. (a) Molecular structure of **3** with thermal ellipsoids rendered at the 50% probability level. Hydrogen atoms are omitted for clarity. Color scheme: iron, orange; phosphorus, yellow; nitrogen, blue; carbon, gray; oxygen, red. (b) Superposition of the molecular structures of **1** (blue, CCDC 978092) and **3** (red).

($\sim1°$) relative to **1**. This modest perturbation is illustrated by the structural overlay of **1** and **3** shown in Figure 2b. The slight expansion of the Fe−Fe bond may reasonably be attributed to increased electron density at the iron atoms of **3** as a consequence of aromatic isocyanide substitution for a CO ligand, isocyanides being generally regarded as both stronger σ-donors and weaker π-acids than CO.[19] Note that the pseudolinear configuration of the isocyanide moiety in **3** also contributes to the retention of the structural features observed in **1** by effectively separating the aromatic isocyanide ligand from the steric congestion imposed on the coordination sphere

by the phosphorus-bound phenyl groups and residual CO ligands.

Despite their structural similarities, complexes **1** and **3** exhibit marked differences in their electrochemical responses, as illustrated by the cyclic voltammograms (CVs) presented in Figure 3a. Most notably, the cathodic and anodic peak potentials of complex **1** shift from −1.64 and −1.48 V respectively to −1.81 and −1.72 V in complex **3**. This overall cathodic shift is attributed to more localized electron density at the metal atoms as a result of the weaker π-acidity of the aromatic isocyanide relative to CO (*vide supra*). The cyclic

Table 1. Selected Bond Lengths and Angles for Complexes 1 and 3−5

	1[13]	3	4	5
		distances (Å)		
Fe−Fe	2.6047(6)	2.6375(5)	2.6299(5)	2.621(4)
			2.6299(5)	2.631(4)
				2.636(5)
Fe−P (mean)	2.224(3)	2.225(1)	2.220(5)	2.225(3)
Fe−C_{iso}		1.861(2)	1.850(1)	1.82(2)
			1.850(1)	1.85(2)
				1.88(2)
C_{iso}−N		1.164(2)	1.166(2)	1.13(3)
			1.166(2)	1.15(3)
				1.19(3)
		bond angles (deg)		
C_{ipso}−N−C_{iso}		164.9(1)	172.0(1)	160(2)
			172.0(1)	167(2)
				172(2)
Fe−P−Fe (mean)	71.7(2)	72.68(4)	72.61(1)	72.5(1)

voltammogram of **1** also possesses a somewhat irregular shape in which the peak cathodic and anodic current ratio (i_{pa}/i_{pc}) diverges significantly from unity (∼1.28), while i_{pa}/i_{pc} = 1.03 for **3**.

Simulation of electrochemical processes is widely accepted as one of the most effective tools for investigating electron-transfer mechanisms, and we have utilized simulation methods to better understand the voltammetric responses of **1** and **3**.[20] The simulations shown in Figure 3a (represented by open circles) were generated by assigning initial estimates to each of the relevant kinetic and thermodynamic parameters—i.e., the formal potentials ($E0'$), standard heterogeneous rate constants (k_s), transfer coefficients (α), and diffusion coefficients (D)—appearing in the Butler−Volmer kinetic model and then refining the parameters (tabulated in Figure 3b) by using an iterative Gauss−Newton algorithm in the DigiElch software package, the operational principles of which have been described elsewhere.[20,21] A mechanistic model was assumed

in which **1** and **3** undergo sequential single-electron transfer events to produce their corresponding dianions, which is in agreement with previous theoretical treatments of structurally related species and consistent with the recently adopted IUPAC position that "*simultaneous transfer of more than one electron to or from an electrode is highly improbable*".[10c,22] We also observed that models based on stepwise electron transfer mechanisms resulted in a better fit (i.e., smaller standard deviation, S) than alternative models in which a simultaneous two-electron transfer process is assumed.

As one might expect from systems exhibiting potential inversion, the kinetic and thermodynamic parameters are extensively correlated, precluding their quantitative determination using the Gauss−Newton fitting algorithm; consequently, the simulation parameters reported throughout this work are best considered as *plausible* estimates.[23] Parameter coupling notwithstanding, it is worth noting that the estimates of $E0'$, k_s, and D obtained by application of the Butler−Volmer model are also in reasonably good agreement with those obtained by using the Marcus−Hush kinetic model for all of the simulations discussed herein (see Figure S1 of the Supporting Information).

After exploring the structural and electrochemical implications of replacing one of the CO ligands of **1** with a monofunctional aromatic isocyanide, we proceeded to conduct a similar study of complex **4**, which was produced by appending two $Fe_2(PPh_2)_2(CO)_5$ fragments to 1,4-phenylene diisocyanide (**2b**). As expected, the molecular structure of **4** (Figure 4a) is very similar to that of **3**, both having comparable Fe−Fe, Fe−P, and Fe−isocyanide bond lengths (see Table 1). The electroactive $Fe_2(PPh_2)_2(CO)_5$ subunits appended to the central aromatic diisocyanide in **4** are indistinguishable from one another in the solid state, there being a crystallographic inversion center located at the centroid of the isocyanide-bearing aromatic ring. Despite sharing the same space group ($P2_1/n$) and many structural similarities with **3**, the anisotropic molecular geometry of **4** gives rise to a series of void channels (∼6 Å in width) along the crystallographic *a*-axis in the solid state, as highlighted in Figure 4b. Analysis of X-ray diffraction

(a)

(b)

Complex **1**	$E^{0'}$ (V)	α	k_s(cm s^{-1})
1 + e$^-$ ⇋ **1**$^-$	-1.745	0.51	0.046
1$^-$ + e$^-$ ⇋ **1**$^{2-}$	-1.411	0.43	0.016
D(cm^2 s^{-1}) = 3.47 x 10^{-6}, S(%) = 2.75			

Complex **3**	$E^{0'}$ (V)	α	k_s(cm s^{-1})
3 + e$^-$ ⇋ **3**$^-$	-1.879	0.49	0.018
3$^-$ + e$^-$ ⇋ **3**$^{2-}$	-1.649	0.49	0.018
D(cm^2 s^{-1}) = 2.69 x 10^{-6}, S(%) = 2.34			

Figure 3. (a) Experimental (solid lines) and simulated (open circles) cyclic voltammograms of **1** (black) and **3** (blue) recorded in 0.25 M [Bu$_4$N][PF$_6$] DMF solutions at ν = 50 mV/s. (b) Kinetic and thermodynamic parameters used to produce each simulation in the DigiElch software package. Diffusion coefficients (D) were assumed equal for each neutral parent complex and the corresponding mono- and dianions. The standard deviations of the data fits, S (%), are indicated.

Figure 4. (a) Molecular structure of **4** with thermal ellipsoids rendered at the 50% probability level. Hydrogen atoms are omitted for clarity. The color scheme is as described in Figure 2. (b) Molecular packing of **4** viewed parallel to the crystallographic *a*-axis. Atoms are depicted at the full van der Waals radius, and the locations of void channels are indicated by blue cylinders.

data leads us to believe that these channels are occupied by highly disordered dichloromethane molecules (see the Supporting Information). Although we have not yet pursued such experiments, these channels would appear to be well-suited for the adsorption of small, nonpolar species such as CO_2, which may be able to displace residual solvent molecules.

In the absence of electronic communication or other energy-perturbing interactions between the electroactive subunits of **4**, one might anticipate that the voltammetric responses of the $Fe_2(PPh_2)_2(CO)_5$ subunits would be identical and appear very similar to the response of **3**, albeit manifesting a larger current contribution reflecting a net transfer of four electrons rather than two (see Figure S2).[24] As shown in Figure 5a, however, splitting of the waves associated with the reduction of the individual $Fe_2(PPh_2)_2(CO)_5$ subunits is observed. This splitting might suggest that (i) the electronic states of the organometallic subunits are coupled to one another via the aromatic isocyanide ligand, (ii) through-space electrostatic repulsions associated with 4^{2-} are responsible for the modest negative shift in the reduction potentials required to generate 4^{4-}, (iii) strong ion-pairing between 4^{2-} and electrolyte cations is responsible for the observed splitting, or (iv) some combination of the former interactions may be at work.[25] Although through-bond coupling of electronic states has been reported for electroactive species connected via a *para*-substituted aromatic core, such coupling is believed to be less efficient when electroactive subunits reside at positions *ortho* or *meta* to one another.[26] Thus, the observation of similar magnitudes of splitting (~100 mV) in the cathodic responses of **4** and **5** (in which all the electroactive subunits lie at *meta* positions; *vide infra*) might be taken as evidence that the splitting observed in Figure 5a is not predominantly a consequence of through-bond electronic coupling.

Simulation of the voltammetric response (represented by open circles in Figure 5a) was once again used to lend support to the proposed mechanism of electron transfer in which **4** undergoes four single-electron transfer events, the second and fourth of which are characterized by potential inversions. The relevant kinetic and thermodynamic parameters used to produce reasonable simulated facsimiles of the original experimental voltammograms are tabulated in Figure 5b.

Having prepared a noncanonical cluster (**4**) capable of accommodating four electrons, we were determined to extend the modular assembly strategy to produce a noncanonical cluster whose electron-sink capacity might rival those of the benchmark canonical clusters $[Ni_{32}C_6(CO)_{36}]^{6-}$ and $[Ni_{38}Pt_6(CO)_{48}]^{6-}$, each of which is known to accommodate up to five electrons per molecule.[4] To this end, we combined

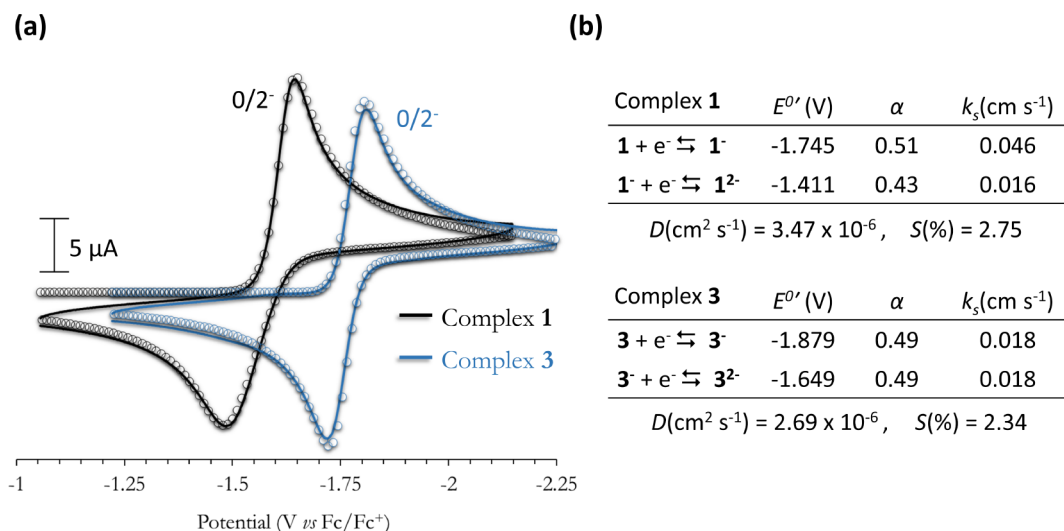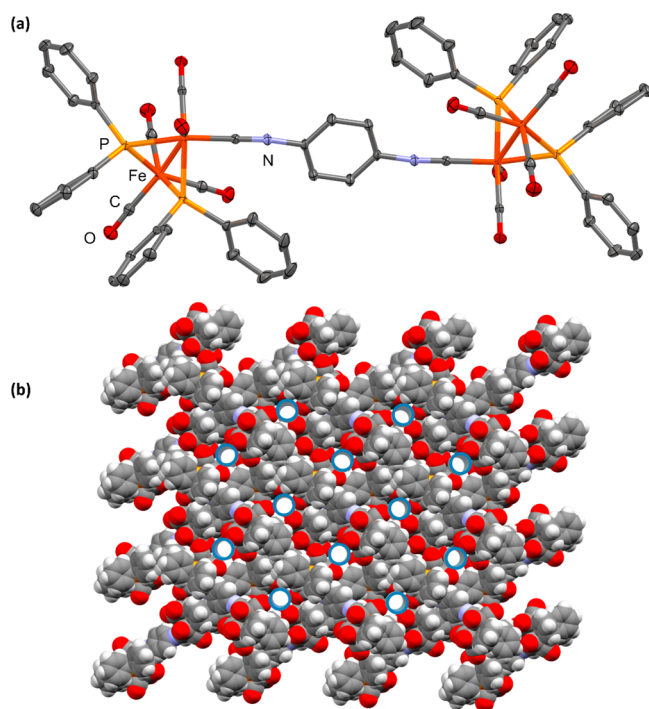**Figure 5.** (a) Experimental (solid line) and simulated (open circles) cyclic voltammograms of **4** (1 mM) recorded in a 0.25 M $[Bu_4N][PF_6]$ DMF solution at ν = 50 mV/s. (b) Kinetic and thermodynamic parameters used in the simulation. The diffusion coefficient (D) was assumed equal for **4** and each of the ions appearing in the proposed mechanism.

	$E^{0\prime}$ (V)	α	k_s (cm s^{-1})
4 + e$^-$ ⇆ **4**$^-$	-1.822	0.67	0.012
4$^-$ + e$^-$ ⇆ **4**$^{2-}$	-1.438	0.46	0.012
4^{2-} + e$^-$ ⇆ **4**$^{3-}$	-2.091	0.44	0.083
4^{3-} + e$^-$ ⇆ **4**$^{4-}$	-1.525	0.48	0.10

$$D\,(\text{cm}^2\,\text{s}^{-1}) = 1.63 \times 10^{-6}, \quad S(\%) = 3.45$$

1-NCMe with aromatic triisocyanide **2c** to produce **5**, the synthesis of which was conveniently performed at the gram scale.

Many attempts were made to grow single crystals of **5** suitable for X-ray diffraction studies, most resulting in the precipitation of fine powders or glassy, amorphous residues. The highest-quality crystals were grown by slow diffusion of isopropanol vapor into a concentrated solution of **5** in toluene. The structural solution and refinement of **5** was complicated by the presence of approximately nine disordered toluene molecules within the asymmetric unit, only three of which could be modeled satisfactorily. Despite these challenges, the molecular structure of **5** was eventually determined, as shown in Figure 6.

Figure 6. Molecular structure of **5** with thermal ellipsoids rendered at the 50% probability level. Hydrogen atoms are omitted for clarity. The color scheme is as described in Figure 2.

Inspection of Figure 6 and the relevant entries in Table 1 reveals that the $Fe_2(PPh_2)_2(CO)_5$ subunits of **5** are not materially distorted compared to those of compounds **3** and **4**, despite being brought nearer to one another via tethering to isocyanide functional groups residing at the *meta*-positions of the aromatic hub. Once again, the pseudolinear configuration of the isocyanide moiety may be credited with relieving steric congestion between the $Fe_2(PPh_2)_2(CO)_5$ subunits by acting as a radial spacer relative to the plane of the central mesitylene ring. Moreover, the observation of three different bond angles (160°, 167°, and 172°) between the ipso carbons of the arylisocyanide ring and the nitrogen and carbon atoms of the isocyanide groups suggests that deformation of the isocyanide moiety also plays a role in relieving steric congestion.

The cyclic voltammogram of **5** (Figure 7a) bears some similarity to that of **4** in that splitting of the voltammetric waves is again observed. Unlike the voltammetric wave of **4**, a third peak is present in the current response, corresponding to the reduction of a third $Fe_2(PPh_2)_2(CO)_5$ subunit and the accumulation of six electrons per molecule. Simulations based on a mechanism of six single-electron transfer events faithfully reproduced the experimental response as long as potential inversions were assumed for the second, fourth, and sixth electron transfers (Figure 7b).

Considering the results of the electrochemical studies of compounds **3** and **4**, it may appear rather obvious that the hexaanion of **5** would be observed in solution under routine experimental conditions; however, such an *a priori* assumption is challenged by literature accounts describing various unconventional experimental conditions that have—of necessity—been used to access the full range of redox states in other electron-sink molecules. For example, the reduction of C_{60} to its hexaanion (C_{60}^{6-}) was performed in a mixed acetonitrile–toluene solvent system at low temperatures and under high vacuum conditions to facilitate the complete reduction of C_{60} without concomitant degradation of the electrolyte solution, the potentials of the six single-electron transfers ranging from approximately −1 to −3 V (vs Fc/Fc$^+$).[27] Similarly, an unusual tetra-*n*-butylammonium fluoroborate toluene solvate, $[NBu^n_4][BF_4]\cdot 3(C_7H_8)$, was employed as both solvent and electrolyte to observe all of the members of the $[Fe_4S_4(SPh)_4]^{1-/2-/3-/4-}$ electron transfer series over a potential range of about 0 to

	$E^{0\prime}$ (V)	α	k_s (cm s^{-1})
5 + e$^-$ ⇆ **5**$^-$	-1.847	0.51	0.028
5$^-$ + e$^-$ ⇆ **5**$^{2-}$	-1.455	0.43	0.011
5^{2-} + e$^-$ ⇆ **5**$^{3-}$	-1.960	0.47	0.022
5^{3-} + e$^-$ ⇆ **5**$^{4-}$	-1.597	0.53	0.011
5^{4-} + e$^-$ ⇆ **5**$^{5-}$	-2.064	0.39	0.012
5^{5-} + e$^-$ ⇆ **5**$^{6-}$	-1.690	0.53	0.022

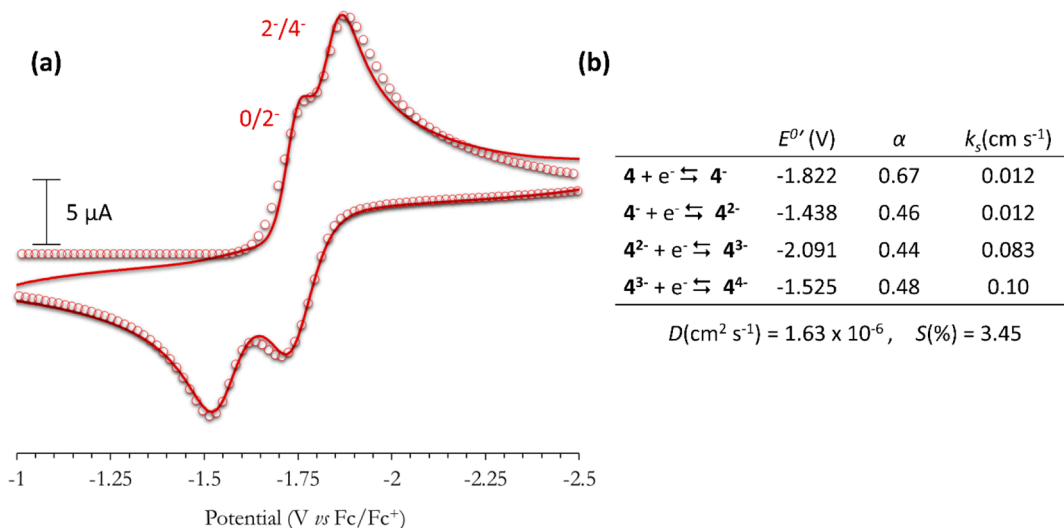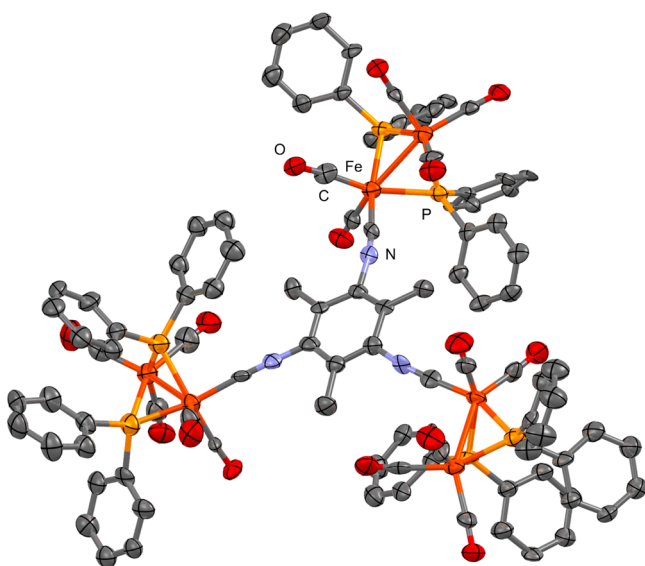D (cm^2 s^{-1}) = 1.83 x 10^{-6}, S(%) = 3.03

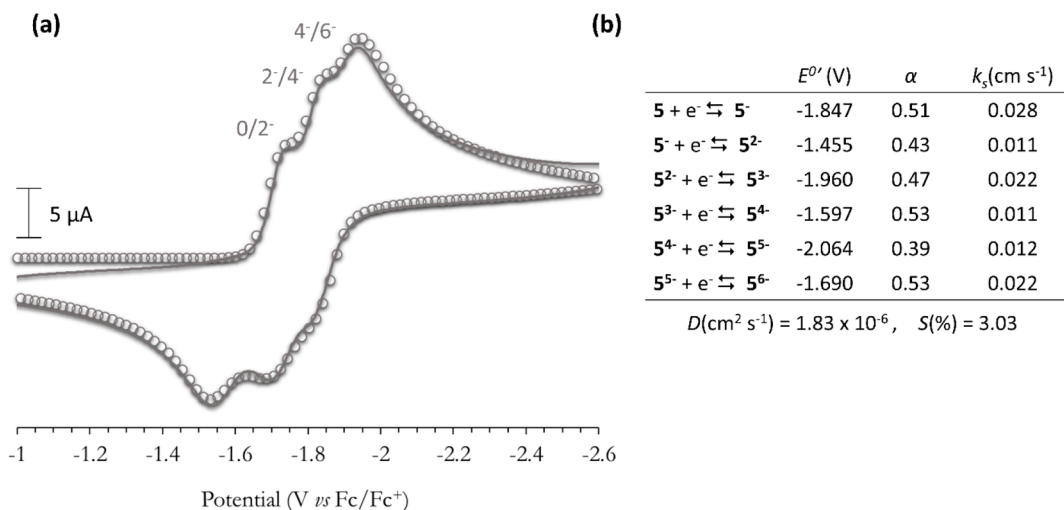**Figure 7.** (a) Experimental (solid line) and simulated (open circles) cyclic voltammograms of **5** (1 mM) recorded in a 0.25 M [Bu$_4$N][PF$_6$] DMF solution at ν = 50 mV/s. (b) Kinetic and thermodynamic parameters used in the simulation. The diffusion coefficient (D) was assumed equal for **5** and each of the ions appearing in the proposed mechanism.

−2.5 V (vs Fc/Fc$^+$).[28] In cases such as these, potential inversion is not operative, and the stepwise addition of each electron drives the potentials of subsequent electron transfers to more negative values. Consequently, the potentials required to completely "charge" a molecule to its full electron-sink capacity can easily exceed the potential window of stability (i.e., the so-called "solvent window") of many common organic electrolyte solutions.[29] By contrast, all five redox states of the benchmark canonical cluster $[Ni_{32}C_6(CO)_{36}]^{6−}$ may be accessed between about −0.8 and −2 V (vs Fc/Fc$^+$), and it is this relatively narrow potential window that makes the large canonical clusters particularly attractive as functional materials.[3e] It is in this context that the electron-sink properties of noncanonical cluster **5** may be fully appreciated: all of its redox states (i.e., **5** to **5**$^{6−}$) are accessible within a potential window of approximately −1.4 to −2.1 V (vs Fc/Fc$^+$), the range having been substantially compressed by virtue of the potential inversion for the addition of the second, fourth, and sixth electrons. A similar potential compression was reported by Wang et al. for a diiron dithiolate complex consisting of three $Fe_2S_2(CO)_6$ subunits sharing a common benzenehexathiolate core.[7] The potential window over which the latter experienced complete cathodic charging was slightly wider (∼0.9 V) than that of complex **5**, resulting in increased separation between each of the cathodic peaks. This separation allowed the authors to electrolyze the complex at various potential intervals and study the reduction products in a stepwise manner without resorting to simulation and model fitting techniques to probe the mechanistic details of electron transfer.

CONCLUSIONS

The objective of this study was to develop a modular synthetic strategy whereby organometallic complexes with significant and predictable electron-sink capacity might be assembled by using only a handful of readily accessible molecular components. By exploiting the two-electron reduction capacity of the $Fe_2(PPh_2)_2(CO)_5$ fragment and its affinity toward isocyanide functional groups, the electron-sink capacity of modularly assembled complexes prepared therefrom was deliberately expanded from two electrons in the parent complex to four or six electrons in *noncanonical cluster assemblies*—so designated because they exhibit electron-sink properties similar to those of large multinuclear clusters yet lack the central metallic core and extensive metal−metal bonding typifying the latter (e.g., $[Ni_{32}C_6(CO)_{36}]^{6−}$ and $[Ni_{38}Pt_6(CO)_{48}]^{6−}$).

Notably, the assembly bearing three $Fe_2(PPh_2)_2(CO)_5$ fragments (**5**) underwent reduction to a hexaanionic state over a potential range of about −1.4 to −2.1 V (vs Fc/Fc$^+$), well within the stability window of common organic electrolyte solutions. Electrochemical simulations based on a mechanism of sequential single-electron transfer events satisfactorily reproduced the experimental voltammetric responses only if potential inversion was assumed to be operative during the addition of the second, fourth, and sixth electrons, and it is this potential inversion that enables the noncanonical cluster to achieve full cathodic "charging" with six electrons over a relatively compressed potential range (∼0.7 V). Although the voltammetric behavior of complexes **3**, **4**, and **5** has been extensively characterized and the mechanisms of electron transfer elucidated, isolation of the corresponding anions has proven challenging; as such, a study of the bulk electro-

chemical properties of **3**, **4**, and **5** (and their respective anions) could represent an interesting avenue for future research.

The present study has explored the modular preparation of noncanonical clusters based on the $Fe_2(PPh_2)_2(CO)_5$ fragment, but we expect that the strategy should be extendable to other transition-metal-based electron-sink compounds, particularly other 34-electron species such as the diiron dithiolato carbonyl complexes or the dinuclear carbonyl complexes of Mo and W bearing dithiolato or diphosphido moieties.[30] One might further speculate that species like **5**, capable of progressing from a charge-neutral to highly anionic state, might be used in parallel with complementary species capable of accessing highly cationic states—such as the "superatoms" reported by Nuckolls et al.[8]—to fabricate molecular-scale charge storage systems. Conveniently, the noncanonical clusters described in this work retain the phosphorus-bound aromatic rings of the parent $Fe_2(PPh_2)_2(CO)_6$ complex, which might lend themselves to future chemical modifications that could facilitate the grafting of the noncanonical clusters to electrode surfaces, producing capacitive materials with interesting properties.

■ EXPERIMENTAL SECTION

General Considerations. All reactions were performed by using standard Schlenk techniques under an inert nitrogen atmosphere. Nitrogen gas was purified by passage through columns of activated copper catalyst (BASF PuriStar R3-11G) and molecular sieves (RCI-DRI 13X). All solvents were dried according to standard procedures.[31] Glassware was dried in an oven at 130 °C, assembled while hot, and allowed to cool under reduced pressure. Formic acid (Beantown Chemical, 99%), acetic anhydride (Beantown Chemical, 99%), POCl$_3$ (Acros, 99%), and trimethylamine *N*-oxide dihydrate (Beantown Chemical, 98%) were used as received without further purification. $[Bu_4N][PF_6]$ (CHEM-IMPEX INT'L INC., 98.48%) was recrystallized before use. $Fe_2(PPh_2)_2(CO)_6$ (**1**) may be synthesized either by the method of Collman et al.[9a] or the modified synthesis described by Wojcicki et al.[9b] 2,4,6-Triaminomesitylene, 2,6-dimethylphenyl isocyanide (**2a**), and 1,4-phenylene diisocyanide (**2b**) were prepared according to published procedures.[16,32]

Infrared spectra were collected by using a Thermo Scientific Nicolet iS5 FT-IR spectrometer equipped with a BaF$_2$ liquid cell with a 0.2 mm fluid channel. ^{1}H and ^{13}C NMR spectra were obtained by using a 600 MHz Bruker AVANCE III spectrometer. High-resolution electrospray ionization mass spectrometry (ESI-MS) was performed on a Thermo Scientific Exactive Plus Orbitrap mass spectrometer (additional details available in the Supporting Information). Elemental analyses were performed by Atlantic Microlab, Inc. (Norcross, GA).

Synthesis of 2,4,6-Triformamidomesitylene. Formic acid (4.97 mL, 132 mmol) was combined with acetic anhydride (99%, 4.48 mL, 47.0 mmol) and magnetically stirred at 0 °C for 20 min. 2,4,6-Triaminomesitylene (2.07 g, 12.5 mmol) was dissolved in 70 mL of CH$_2$Cl$_2$ and was slowly introduced to the reaction flask via a syringe. The combined mixture was magnetically stirred at 0 °C for 20 min and then stirred for an additional 24 h at 25 °C, after which the mixture thickened and assumed a pale yellow color. Solvents were removed under reduced pressure, and a pale yellow solid was obtained. The solid was suspended in cold methanol, filtered, and washed with additional cold methanol. The solid was then dried under reduced pressure at 50 °C for 1 h, and the product was obtained as a white powder. Yield: 2.55 g (81.6%). IR (ATR, cm^{-1}): 3174 (w), 3013 (w), 2913 (w), 1651 (ν_{CO}, s), 1587 (m), 1533 (m), 1495 (m). ^{13}C NMR (600 MHz, DMSO-d_6): δ 14.2, 131.2, 132.3, 159.6. Note: ^{1}H NMR is complicated by the presence of *cis* and *trans* tautomeric isomers. MS (ESI): *m/z* 272.10 [M + Na]$^+$, 288.07 [M + K]$^+$. Anal. Calcd for C$_{12}$H$_{15}$N$_3$O$_3$: C, 57.82; H, 6.07; N, 16.86. Found: C, 57.67; H, 6.11; N, 16.76.

Synthesis of 2,4,6-Triisocyanomesitylene (2c). 2,4,6-Triformamidomesitylene (1.02 g, 4.09 mmol) and triethylamine (5 mL) were combined in 100 mL of CH₂Cl₂. The pale yellow suspension was magnetically stirred while POCl₃ (2.26 g, 14.7 mmol) was added dropwise, whereupon the solution assumed a hazy orange color. The reaction mixture was then heated at reflux for 6 h and stirred for an additional 24 h at 25 °C. The reaction mixture was quenched with a saturated aqueous sodium bicarbonate solution, and the biphasic mixture was filtered to remove insoluble impurities. The aqueous layer was extracted twice with CH₂Cl₂, and the organic extract was dried over anhydrous MgSO₄. The crude solid was then purified by vacuum sublimation (9.7 Torr) at 80 °C. Yield: 0.493 g (61.8%). The spectroscopic data were consistent with published values.[17]

Synthesis of Fe₂(PPh₂)₂(CO)₅(NCCH₃) (1-NCMe). Using a modified version of the procedure reported by Mizuta et al.,[18] 1 (2.01 g, 3.10 mmol) was dissolved in 70 mL of CH₃CN, followed by addition of TMANO (1.18 g, 10.6 mmol). The bright red reaction mixture was magnetically stirred at 50 °C for 2 h, becoming opaque after about 10 min. The solvent was removed under reduced pressure, and the resulting red residues were suspended in CH₂Cl₂ and filtered through a short pad of activated alumina (60 mesh) to remove insoluble impurities. The filtrate was collected and dried under reduced pressure, leaving a flaky red solid that was used in subsequent steps without further purification. Yield: 1.73 g (84.3%). IR (CH₂Cl₂, cm⁻¹): ν_{CO} 2023 (m), 1980 (s), 1941 (m), 1921 (w).

Synthesis of Complex 3. 1-NCMe (0.416 g, 627 mmol) was dissolved in THF (20 mL), after which 2a (0.0822 g, 627 mmol) was added, and the mixture stirred for 5 h at 50 °C. The solvent was removed under reduced pressure, and the crude product was dissolved in toluene and filtered through a short pad of silica gel. The filtrate was dried under reduced pressure, and the resulting red solid was recrystallized from acetonitrile at −20 °C. Yield: 364 mg (77.1%). Single crystals suitable for X-ray diffraction studies were obtained by slow diffusion of ethanol vapor into a concentrated solution of 3 in acetonitrile. IR (toluene, cm⁻¹): ν_{CN} 2109 (m), ν_{CO} 2025 (s), 1986 (s), 1966 (w), 1948 (s), 1937 (m). ¹H NMR (600 MHz, CDCl₃): δ 2.06 (s, 6 H), 6.69 (t, 4 H), 6.79 (t, 2 H), 6.97 (d, 2 H), 7.04 (t, 1 H), 7.17 (m, 11 H), 7.64 (m, 4 H). Anal. Calcd for C₃₈H₂₉Fe₂NO₅P₂: C, 60.59; H, 3.88; N, 1.86. Found: C, 60.66; H, 3.90; N, 1.93. MS (ESI): m/z 784.04 [M + MeO]⁻.

Synthesis of Complex 4. 1-NCMe (0.340 g, 0.513 mmol) was dissolved in THF (30 mL), followed by addition of 1,4-phenylene diisocyanide (2b) (0.0285 g, 0.222 mmol). The mixture was magnetically stirred for 3 h at 50 °C, after which the solvent was removed under reduced pressure. The resulting residues were dissolved in CH₂Cl₂ and filtered through a short pad of silica gel, after which the filtrate was dried under vacuum. Red crystals were isolated by layering methanol on top of a concentrated solution of 4 and allowing the solvents to mix by diffusion. Yield: 0.188 g (61.7%). IR (toluene, cm⁻¹) ν_{CN} 2104 (m, br), ν_{CO} 2023 (m), 1988 (s), 1966 (w), 1949 (s). ¹H NMR (600 MHz, CD₂Cl₂), δ 6.33 (s, 4 H), 6.71 (t, 8 H), 6.81 (t, 4 H), 7.18 (m, 9 H), 7.23 (m, 12 H), 7.69 (m, 8 H). Anal. Calcd for C₆₆H₄₄Fe₄N₂O₁₀P₄: C, 57.76; H, 3.23; N, 2.01. Found: C, 57.49; H, 3.33; N, 2.14. MS (ESI): m/z 1402.97 [M + MeO]⁻.

Synthesis of Complex 5. 1-NCMe (1.70 g, 2.56 mmol) and 2,4,6-triisocyanomesitylene (2c) (0.139 g, 0.712 mmol) were dissolved in THF (100 mL), and the reaction mixture was magnetically stirred for 3 h at 50 °C, after which the solvent was removed under reduced pressure. The remaining red residues were extracted into CH₂Cl₂ and filtered through a short pad of silica gel. The filtrate was dried under vacuum, and the remaining solid was dissolved in hot CH₃CN and slowly cooled to 0 °C, whereupon a fine yellow precipitate formed. The precipitate was filtered, washed with cold CH₃CN, and redissolved in toluene. Layering of isopropanol onto a concentrated solution of 5 in toluene produced red crystals after several days, which were filtered and dried under reduced pressure. The elemental composition of crystals isolated in this manner is consistent with that of a toluene solvate of 5 (C₉₉H₆₉Fe₆N₃O₁₅P₆·0.4C₇H₈). Yield: 1.14 g (76.3%). IR (CH₂Cl₂, cm⁻¹), ν_{CN} 2087 (m, br), ν_{CO} 2022 (s), 1988 (s), 1953 (s). ¹H NMR (600 MHz, CDCl₃), δ 1.68 (s, 9 H), 6.69 (t, 12 H), 6.80 (t, 6 H), 7.15 (m, 12 H), 7.16 (m, 19 H), 7.60 (m, 12 H). Anal. Calcd for C₉₉H₆₉Fe₆N₃O₁₅P₆·0.4 C₇H₈: C, 58.27; H, 3.47; N, 2.00. Found: C, 58.17; H, 3.41; N, 2.06. MS (ESI): m/z 2092.97 [M + MeO]⁻.

Cyclic Voltammetry. Cyclic voltammograms of each electroactive compound were recorded in 0.25 M [Bu₄N][PF₆] DMF solutions (1 mM analyte) by using a Princeton Applied Research PARSTAT 4000A potentiostat. All experiments were performed by using a standard three-electrode configuration under an atmosphere of pure nitrogen. Glassy carbon disk working electrodes (∼3 mm, CH Instruments) were used for all measurements and were sequentially polished with aqueous slurries of 0.3 and 0.05 μm alumina powder prior to use. After polishing, the electrodes were rinsed with Milli-Q water and methanol and dried in a stream of air. Working electrodes were preconditioned by performing three cyclical scans from 1.5 to −2.5 V at 100 mV/s prior to analyte addition. A graphite rod served as the counter electrode and a silver wire immersed in a 0.25 M DMF solution of [Bu₄N][PF₆] and separated from the cell compartment by a porous glass frit (CoralPor 1000) was employed as a Ag⁺/Ag pseudoreference electrode. Measured potentials are reported relative to the ferrocenium(1+)/ferrocene(0) redox couple. Uncompensated resistance (R_u) was determined by electrochemical impedance spectroscopy, and an iR_u drop correction was applied by using the instrument's positive feedback feature to compensate for 90% of the measured value of R_u.

Digital simulations and data fitting were carried out by using the DigiElch software package, Ver. 8.0 (see the Supporting Information).

Controlled Potential Coulometry. Coulometric measurements were performed in 0.25 M [Bu₄N][PF₆] DMF solutions under an atmosphere of pure nitrogen by using a Princeton Applied Research PARSTAT 4000A potentiostat. A three-electrode cell consisting of a Hg pool working electrode, a coiled platinum wire counter electrode, and a Ag⁺/Ag pseudoreference electrode was used for all experiments. The counter electrode was immersed in a 0.25 M [Bu₄N][PF₆] DMF solution that had been saturated with ferrocene and was separated from the working electrode chamber by a porous glass frit. Solutions of electroactive compounds 3, 4, and 5 (each ∼1 mM) were exhaustively electrolyzed at potentials approximately 200 mV negative of the peak cathodic potential observed in their respective cyclic voltammograms until a constant current was observed. Although the results of the controlled potential coulometry experiments performed under cathodic conditions were consistent with the accumulation of two, four, and six electrons for compounds 3, 4, and 5, respectively, cyclic voltammograms obtained before and after electrolysis suggested that bulk reduction over mercury induced degradation of the reduced products (see Figure S7). Consequently, controlled potential coulometry experiments could not be performed in the reverse (anodic) direction. Several attempts were made to isolate the products of electrolysis, but efforts were hampered by extreme air sensitivity of the reduced species under the experimental conditions described above.

■ ASSOCIATED CONTENT

Ⓢ Supporting Information

The Supporting Information is available free of charge at https://pubs.acs.org/doi/10.1021/acs.inorgchem.1c02373.

> Supplementary electrochemical data and simulations, information about X-ray diffraction methods and data refinement, ESI-MS methods and data, IR spectra, and ¹³C and ¹H NMR spectra (PDF)

Accession Codes

CCDC 2101487−2101489 contain the supplementary crystallographic data for this paper. These data can be obtained free of charge via www.ccdc.cam.ac.uk/data_request/cif, or by emailing data_request@ccdc.cam.ac.uk, or by contacting The

Cambridge Crystallographic Data Centre, 12 Union Road, Cambridge CB2 1EZ, UK; fax: +44 1223 336033.

■ AUTHOR INFORMATION

Corresponding Author

Adam C. Colson − *Department of Chemistry and Biochemistry, Boise State University, Boise, Idaho 83725, United States;* ⊙ orcid.org/0000-0002-1114-7791; Email: adamcolson@boisestate.edu

Authors

Yume Mai − *Department of Chemistry and Biochemistry, Boise State University, Boise, Idaho 83725, United States*

Alexandria K. Balzen − *Department of Chemistry and Biochemistry, Boise State University, Boise, Idaho 83725, United States*

Rebecca K. Torres − *Department of Chemistry and Biochemistry, Boise State University, Boise, Idaho 83725, United States*

Michael P. Callahan − *Department of Chemistry and Biochemistry, Boise State University, Boise, Idaho 83725, United States*

Complete contact information is available at:
https://pubs.acs.org/10.1021/acs.inorgchem.1c02373

Notes

The authors declare no competing financial interest.

■ REFERENCES

(1) (a) Kumar, Y.; Rawal, S.; Joshi, B.; Hashmi, S. A. Background, fundamental understanding and progress in electrochemical capacitors. *J. Solid State Electrochem.* **2019**, *23*, 667−692. (b) Wang, Y.; Song, Y.; Xia, Y. Electrochemical capacitors: mechanism, materials, systems, characterization and applications. *Chem. Soc. Rev.* **2016**, *45*, 5925−5950. (c) Zhang, Y.; Feng, H.; Wu, X.; Wang, L.; Zhang, A.; Xia, T.; Dong, H.; Li, X.; Zhang, L. Progress of electrochemical capacitor electrode materials: A review. *Int. J. Hydrogen Energy* **2009**, *34*, 4889−4899. (d) Marchante, E.; Maglione, M. S.; Crivillers, N.; Rovira, C.; Mas-Torrent, M. A four-state capacitance molecular switch based on a redox active tetrathiafulvalene self-assembled monolayer. *RSC Adv.* **2017**, *7*, 5636−5641. (e) Lindsey, J. S.; Bocian, D. F. Molecules for Charge-Based Information Storage. *Acc. Chem. Res.* **2011**, *44*, 638−650. (f) Auwärter, W.; Écija, D.; Klappenberger, F.; Barth, J. V. Porphyrins at interfaces. *Nat. Chem.* **2015**, *7*, 105. (g) Mas-Torrent, M.; Rovira, C.; Veciana, J. Surface-Confined Electroactive Molecules for Multistate Charge Storage Information. *Adv. Mater.* **2013**, *25*, 462−468. (h) Padmaja, K.; Youngblood, W. J.; Wei, L.; Bocian, D. F.; Lindsey, J. S. Triple-Decker Sandwich Compounds Bearing Compact Triallyl Tripods for Molecular Information Storage Applications. *Inorg. Chem.* **2006**, *45*, 5479−5492. (i) Meng, F.; Hervault, Y.-M.; Shao, Q.; Hu, B.; Norel, L.; Rigaut, S.; Chen, X. Orthogonally modulated molecular transport junctions for resettable electronic logic gates. *Nat. Commun.* **2014**, *5*, 3023. (j) Bueno, P. R. Common Principles of Molecular Electronics and Nanoscale Electrochemistry. *Anal. Chem.* **2018**, *90*, 7095−7106.

(2) (a) Echegoyen, L.; Echegoyen, L. E. Electrochemistry of Fullerenes and Their Derivatives. *Acc. Chem. Res.* **1998**, *31*, 593−601. (b) Tran, N. E.; Lambrakos, S. G.; Lagowski, J. J. Analysis of Capacitance Characteristics of C_{60}, C_{70}, and La@C_{82}. *J. Mater. Eng. Perform.* **2009**, *18*, 95−101. (c) Cerón, M. R.; Zhan, C.; Campbell, P. G.; Freyman, M. C.; Santoyo, C.; Echegoyen, L.; Wood, B. C.; Biener, J.; Pham, T. A.; Biener, M. M. Integration of Fullerenes as Electron Acceptors in 3D Graphene Networks: Enhanced Charge Transfer and Stability through Molecular Design. *ACS Appl. Mater. Interfaces* **2019**, *11*, 28818−28822. (d) Schon, T. B.; DiCarmine, P. M.; Seferos, D. S. Polyfullerene Electrodes for High Power Supercapacitors. *Adv. Energy Mater.* **2014**, *4*, 1301509. (e) Shukla, J.; Singh, V. P.; Mukhopadhyay, P. Molecular and Supramolecular Multiredox Systems. *ChemistryOpen* **2020**, *9*, 304−324. (f) Striepe, L.; Baumgartner, T. Viologens and Their Application as Functional Materials. *Chem. - Eur. J.* **2017**, *23*, 16924−16940. (g) Benniston, A. C.; Hagon, J.; He, X.; Yang, S.; Harrington, R. W. Spring Open Two-plus-Two Electron Storage in a Disulfide-Strapped Methyl Viologen Derivative. *Org. Lett.* **2012**, *14*, 506−509. (h) Shukla, J.; Mukhopadhyay, P. Synthesis of Functionalized Naphthalene Diimides and their Redox Properties. *Eur. J. Org. Chem.* **2019**, *2019*, 7770−7786. (i) Shukla, J.; Ajayakumar, M. R.; Kumar, Y.; Mukhopadhyay, P. Electron sponge from naphthalenediimide−viologen conjugates: water-stable, highly electron-deficient polyions with 1 V potential window. *Chem. Commun.* **2018**, *54*, 900−903. (j) Wang, H.; Hamanaka, S.; Nishimoto, Y.; Irle, S.; Yokoyama, T.; Yoshikawa, H.; Awaga, K. Operando X-ray Absorption Fine Structure Studies of Polyoxometalate Molecular Cluster Batteries: Polyoxometalates as Electron Sponges. *J. Am. Chem. Soc.* **2012**, *134*, 4918−4924. (k) Li, Q.; Zhang, L.; Dai, J.; Tang, H.; Li, Q.; Xue, H.; Pang, H. Polyoxometalate-based materials for advanced electrochemical energy conversion and storage. *Chem. Eng. J.* **2018**, *351*, 441−461. (l) Astruc, D. From Electron-Reservoir Complexes to Dendritic Molecular Nanobatteries. *Chem. - Asian J.* **2011**, *6*, 1679−1687. (m) Astruc, D. Electron-reservoir complexes and other redox-robust reagents: functions and applications. *New J. Chem.* **2009**, *33*, 1191−1206. (n) Liu, X.; Rapakousiou, A.; Deraedt, C.; Ciganda, R.; Wang, Y.; Ruiz, J.; Gu, H.; Astruc, D. Multiple applications of polymers containing electron-reservoir metal-sandwich complexes. *Chem. Commun.* **2020**, *56*, 11374−11385. (o) Benson, C. R.; Hui, A. K.; Parimal, K.; Cook, B. J.; Chen, C.-H.; Lord, R. L.; Flood, A. H.; Caulton, K. G. Multiplying the electron storage capacity of a bis-tetrazine pincer ligand. *Dalton Trans* **2014**, *43*, 6513−6524. (p) Wang, D.-Y.; Liu, R.; Guo, W.; Li, G.; Fu, Y. Recent advances of organometallic complexes for rechargeable batteries. *Coord. Chem. Rev.* **2021**, *429*, 213650.

(3) (a) Schmid, G. Large clusters and colloids. Metals in the embryonic state. *Chem. Rev.* **1992**, *92*, 1709−1727. (b) Johnson, B. F. G. From clusters to nanoparticles and catalysis. *Coord. Chem. Rev.* **1999**, *190−192*, 1269−1285. (c) Thimmappa, B. H. S. Low valent metal clusters — an overview. *Coord. Chem. Rev.* **1995**, *143*, 1−34. (d) Hogarth, G.; Kabir, S. E.; Nordlander, E. Cluster chemistry in the Noughties: new developments and their relationship to nanoparticles. *Dalton Trans* **2010**, *39*, 6153−6174. (e) Femoni, C.; Iapalucci, M. C.; Kaswalder, F.; Longoni, G.; Zacchini, S. The possible role of metal carbonyl clusters in nanoscience and nanotechnologies. *Coord. Chem. Rev.* **2006**, *250*, 1580−1604. (f) Longoni, G.; Femoni, C.; Iapalucci, M. C.; Zanello, P. Electron-Sink Features of Homoleptic Transition-Metal Carbonyl Clusters. In *Metal Clusters in Chemistry*; Braunstein, P., Oro, L. A., Raithby, P. R., Eds.; Wiley-VCH Verlag GmbH: 1999; pp 1137−1158. (g) Rossi, F.; Zanello, P. Electron Reservoir Activity of High-Nuclearity Transition Metal Carbonyl Clusters. *Port. Electrochim. Acta* **2011**, *29*, 309−327.

(4) (a) Calderoni, F.; Demartin, F.; Fabrizi de Biani, F.; Femoni, C.; Iapalucci, M. C.; Longoni, G.; Zanello, P. Electron-Sink Behaviour of the Carbonylnickel Clusters $[Ni_{32}C_6(CO)_{36}]^{6-}$ and $[Ni_{38}C_6(CO)_{42}]^{6-}$: Synthesis and Characterization of the Anions $[Ni_{32}C_6(CO)_{36}]^{n-}$ (n = 5−10) and $[Ni_{38}C_6(CO)_{42}]^{n-}$ (n = 5−9) and Crystal Structure of $[PPh_3Me]_6[Ni_{32}C_6(CO)_{36}] \cdot 4$ MeCN. *Eur. J. Inorg. Chem.* **1999**, *1999*, 663−671. (b) Fabrizi de Biani, F.; Femoni, C.; Iapalucci, M. C.; Longoni, G.; Zanello, P.; Ceriotti, A. Redox Behavior of $[H_{6-n}Ni_{38}Pt_6(CO)_{48}]^{n-}$ (n = 4−6) Anions:A Series of

Metal Carbonyl Clusters Displaying Electron -SinkFeatures. *Inorg. Chem.* **1999**, *38*, 3721−3724.

(5) (a) Braunstein, P.; Oro, L. A.; Raithby, P. R. *Metal Clusters in Chemistry*; Wiley-VCH: Weinheim, Germany, 1999. (b) Shriver, D. F.; Kaesz, H. D.; Adams, R. D. *The Chemistry of Metal Cluster Complexes*; VCH: New York, 1990. (c) Dyson, P. J.; McIndoe, J. S. *Transition Metal Carbonyl Cluster Chemistry*; Gordon and Breach: Amsterdam, 2000. (d) Whitmire, K. H. Main Group−Transition Metal Cluster Compounds of the Group 15 Elements. In *Advances in Organometallic Chemistry*; Stone, F. G. A., Robert, W., Eds.; Academic Press: 1998; Vol. 42, pp 1−145. (e) Zacchini, S. Using Metal Carbonyl Clusters To Develop a Molecular Approach towards Metal Nanoparticles. *Eur. J. Inorg. Chem.* **2011**, *2011*, 4125−4145. (f) Koutsantonis, G. A. Organo-transition metal cluster complexes. In *Organometallic Chemistry*; Fairlamb, I. J. S., Lynam, J. M., Eds.; The Royal Society of Chemistry: 2014; Vol. 39, pp 210−237.

(6) (a) Cotton, F. A. Transition-metal compounds containing clusters of metal atoms. *Q. Rev., Chem. Soc.* **1966**, *20*, 389−401. (b) Cotton, F. A. Strong homonuclear metal-metal bonds. *Acc. Chem. Res.* **1969**, *2*, 240−247.

(7) (a) Chen, L.; Wang, M.; Gloaguen, F.; Zheng, D.; Zhang, P.; Sun, L. Tetranuclear Iron Complexes Bearing Benzenetetrathiolate Bridges as Four-Electron Transformation Templates and Their Electrocatalytic Properties for Proton Reduction. *Inorg. Chem.* **2013**, *52*, 1798−1806. (b) Chen, L.; Wang, M.; Gloaguen, F.; Zheng, D.; Zhang, P.; Sun, L. Multielectron-Transfer Templates via Consecutive Two-Electron Transformations: Iron−Sulfur Complexes Relevant to Biological Enzymes. *Chem. - Eur. J.* **2012**, *18*, 13968−13973.

(8) Champsaur, A. M.; Velian, A.; Paley, D. W.; Choi, B.; Roy, X.; Steigerwald, M. L.; Nuckolls, C. Building Diatomic and Triatomic Superatom Molecules. *Nano Lett.* **2016**, *16*, 5273−5277.

(9) (a) Collman, J. P.; Rothrock, R. K.; Finke, R. G.; Moore, E. J.; Rose-Munch, F. Role of the metal-metal bond in transition-metal clusters. Phosphido-bridged diiron carbonyl complexes. *Inorg. Chem.* **1982**, *21*, 146−156. (b) Yu, Y. F.; Wojcicki, A.; Calligaris, M.; Nardin, G. Synthesis and x-ray crystallographic characterization of the binuclear iron complexes cyclic $(CO)_3Fe(\mu\text{-}PPh_2)(\eta^2\text{-}(C,P)\text{-}\mu\text{-}CH\text{-}(CN)PPh_2)Fe(CO)_3$ and cyclic $(CO)_3Fe(\mu\text{-}PPh_2)(\eta^2\text{-}(P,P')\text{-}\mu\text{-}Ph_2PC(CN)PPh_2)Fe(CO)_3$. *Organometallics* **1986**, *5*, 47−53.

(10) (a) Uhrhammer, D.; Schultz, F. A. Energetics of Concerted Two-Electron Transfer and Metal−Metal Bond Cleavage in Phosphido-Bridged Molybdenum and Tungsten Carbonyl Complexes. *J. Phys. Chem. A* **2002**, *106*, 11630−11636. (b) Lord, R. L.; Schultz, F. A.; Baik, M.-H. Two-Electron Redox Energetics in Ligand-Bridged Dinuclear Molybdenum and Tungsten Complexes. *Inorg. Chem.* **2010**, *49*, 4611−4619. (c) Baik, M.-H.; Ziegler, T.; Schauer, C. K. Density Functional Theory Study of Redox Pairs. 1. Dinuclear Iron Complexes That Undergo Multielectron Redox Reactions Accompanied by a Reversible Structural Change. *J. Am. Chem. Soc.* **2000**, *122*, 9143−9154. (d) Cheah, M. H.; Borg, S. J.; Bondin, M. I.; Best, S. P. Electrocatalytic Proton Reduction by Phosphido-Bridged Diiron Carbonyl Compounds:Distant Relations to the H -Cluster? *Inorg. Chem.* **2004**, *43*, 5635−5644.

(11) Evans, D.; Juusola, P.; Minkkinen, P.; Olsen, C.; Søtofte, I.; Francis, G.; Szunyog, J.; Langstrom, B. The Kinetic Burden of Potential Inversion in Two-Electron Electrochemical Reactions. *Acta Chem. Scand.* **1998**, *52*, 194−197.

(12) Ginsburg, R. E.; Rothrock, R. K.; Finke, R. G.; Collman, J. P.; Dahl, L. F. The (metal-metal)-nonbonding$[Fe_2(CO)_6(\mu_2\text{-}PPh_2)2]^{2-}$ dianion. Synthesis, structural analysis of its unusual dimeric geometry, and stereochemical-bonding implications. *J. Am. Chem. Soc.* **1979**, *101*, 6550−6562.

(13) Shi, Y.-C.; Yang, W.; Shi, Y.; Cheng, D.-C. Syntheses, crystal structures, and electrochemical studies of $Fe_2(CO)_6(\mu\text{-}PPh_2)(\mu\text{-}L)$ (L = OH, OPPh₂, PPh₂). *J. Coord. Chem.* **2014**, *67*, 2330−2343.

(14) (a) Wagner, N. L.; Laib, F. E.; Bennett, D. W. Conformational Isomerism in $(p\text{-}RC_6H_4NC)_2W(dppe)_2$:Substantial Structural Changes Resulting from Subtle Differences in the π -Acidityof p -RC6H₄NC. *J. Am. Chem. Soc.* **2000**, *122*, 10856−10867. (b) Carpen-

ter, A. E.; Mokhtarzadeh, C. C.; Ripatti, D. S.; Havrylyuk, I.; Kamezawa, R.; Moore, C. E.; Rheingold, A. L.; Figueroa, J. S. Comparative Measure of the Electronic Influence of Highly Substituted Aryl Isocyanides. *Inorg. Chem.* **2015**, *54*, 2936−2944. (c) Barybin, M. V.; Meyers, Jr., J. J.; Neal, B. M. Renaissance of Isocyanoarenes as Ligands in Low-Valent Organometallics. In *Isocyanide Chemistry*; pp 493−529. (d) Weber, L. Homoleptic Isocyanide Metalates. *Angew. Chem., Int. Ed.* **1998**, *37*, 1515−1517. (e) Vogler, A. Chapter 10 - Coordinated Isonitriles. In *Organic Chemistry*; Ugi, I., Ed.; Elsevier: 1971; Vol. 20, pp 217−233.

(15) (a) Hahn, F. E. The Coordination Chemistry of Multidentate Isocyanide Ligands. *Angew. Chem., Int. Ed. Engl.* **1993**, *32*, 650−665. (b) Tannenbaum, R. Three-Dimensional Coordination Polymers of Ruthenium(2+) with 1,4-Diisocyanobenzene Ligands and Their Catalytic Activity. *Chem. Mater.* **1994**, *6*, 550−555. (c) Millard, S.; Fothergill, J. W.; Anderson, Z.; Brown, E. C.; King, M. D.; Colson, A. C. Supramolecular Interactions of Group VI Metal Carbonyl Complexes: The Facilitating Role of 1,3-Bis(p-isocyanophenyl)urea. *Inorg. Chem.* **2019**, *58*, 8130−8139. (d) Agnew, D. W.; DiMucci, I. M.; Arroyave, A.; Gembicky, M.; Moore, C. E.; MacMillan, S. N.; Rheingold, A. L.; Lancaster, K. M.; Figueroa, J. S. Crystalline Coordination Networks of Zero-Valent Metal Centers: Formation of a 3-Dimensional Ni(0) Framework with m-Terphenyl Diisocyanides. *J. Am. Chem. Soc.* **2017**, *139*, 17257−17260. (e) Angelici, R. J.; Lazar, M. Isocyanide Ligands Adsorbed on Metal Surfaces: Applications in Catalysis, Nanochemistry, and Molecular Electronics. *Inorg. Chem.* **2008**, *47*, 9155−9165. (f) Nemykin, V. N.; Dudkin, S. V.; Fathi-Rasekh, M.; Spaeth, A. D.; Rhoda, H. M.; Belosludov, R. V.; Barybin, M. V. Probing Electronic Communications in Heterotrinuclear Fe−Ru−Fe Molecular Wires Formed by Ruthenium(II) Tetraphenylporphyrin and Isocyanoferrocene or 1,1′-Diisocyanoferrocene Ligands. *Inorg. Chem.* **2015**, *54*, 10711−10724.

(16) Kamijo, S.; Jin, T.; Yamamoto, Y. Novel Synthetic Route to Allyl Cyanamides:Palladium -CatalyzedCoupling of Isocyanides, Allyl Carbonate, and Trimethylsilyl Azide. *J. Am. Chem. Soc.* **2001**, *123*, 9453−9454.

(17) Huang, Y.-C.; Chen, H.-Y.; Chang, Y.-L.; Vasanthakumar, P.; Chen, S.-Y.; Kao, C.-L.; Wu, C. H.-Y.; Hsu, S. C. N. Synthesis of triisocyanomesitylene β-diketiminato copper(I) complexes and evaluation of isocyanide π-back bonding. *Polyhedron* **2020**, *192*, 114828.

(18) Teramoto, Y.; Kubo, K.; Kume, S.; Mizuta, T. Formation of a Hexacarbonyl Diiron Complex Having a Naphthalene-1,8-bis-(phenylphosphido) Bridge and the Electrochemical Behavior of Its Derivatives. *Organometallics* **2013**, *32*, 7014−7024.

(19) (a) King, R. B.; Saran, M. S. Isocyanide-metal complexes. II. Carbonyl and cyanide stretching modes in tertbutyl isocyanide derivatives of the octahedral metal carbonyls. *Inorg. Chem.* **1974**, *13*, 74−78. (b) Cotton, F. A.; Zingales, F. The Donor-Acceptor Properties of Isonitriles as Estimated by Infrared Study. *J. Am. Chem. Soc.* **1961**, *83*, 351−355. (c) Sarapu, A. C.; Fenske, R. F. Transition metal-isocyanide bond. Approximate molecular orbital study. *Inorg. Chem.* **1975**, *14*, 247−253. (d) Yamamoto, Y. Zerovalent transition metal complexes of organic isocyanides. *Coord. Chem. Rev.* **1980**, *32*, 193−233.

(20) Batchelor-McAuley, C.; Kätelhön, E.; Barnes, E. O.; Compton, R. G.; Laborda, E.; Molina, A. Recent Advances in Voltammetry. *ChemistryOpen* **2015**, *4*, 224−260.

(21) (a) Rudolph, M.; Reddy, D. P.; Feldberg, S. W. A Simulator for Cyclic Voltammetric Responses. *Anal. Chem.* **1994**, *66*, 589A−600A. (b) Rudolph, M. An algorithm of general application for the digital simulation of electrochemical processes. *J. Electroanal. Chem. Interfacial Electrochem.* **1990**, *292*, 1−7. (c) Rudolph, M. A fast implicit finite difference algorithm for the digital simulation of electrochemical processes. *J. Electroanal. Chem. Interfacial Electrochem.* **1991**, *314*, 13−22. (d) Rudolph, M. Digital simulations with the fast implicit finite difference (FIFD) algorithm: Part II. An improved treatment of electrochemical mechanisms with second-order reactions. *J. Electroanal. Chem.* **1992**, *338*, 85−98. (e) Rudolph, M. Digital

simulations with the fast implicit finite-difference (FIFD) algorithm. part 4. Simulation of electrical migration and diffuse double-layer effects. *J. Electroanal. Chem.* **1994**, *375*, 89−99. (f) Rudolph, M. Digital simulation with the fast implicit finite difference (FIFD) algorithm: Part 5: Digital simulations of square wave voltammetry for any user defined electrochemical mechanism comprising first- and second-order chemical reactions. *J. Electroanal. Chem.* **2001**, *503*, 15−27. (g) Rudolph, M. Digital simulations on unequally spaced grids.: Part 1. Critical remarks on using the point method by discretisation on a transformed grid. *J. Electroanal. Chem.* **2002**, *529*, 97−108. (h) Rudolph, M. Digital simulations on unequally spaced grids.: Part 2. Using the box method by discretisation on a transformed equally spaced grid. *J. Electroanal. Chem.* **2003**, *543*, 23−39. (i) Rudolph, M. Digital simulations on unequally spaced grids. Part 3. Attaining exponential convergence for the discretisation error of the flux as a new strategy in digital simulations of electrochemical experiments. *J. Electroanal. Chem.* **2004**, *571*, 289−307. (j) Rudolph, M. Attaining exponential convergence for the flux error with second- and fourth-order accurate finite-difference equations. I. Presentation of the basic concept and application to a pure diffusion system. *J. Comput. Chem.* **2005**, *26*, 619−632. (k) Rudolph, M. Attaining exponential convergence for the flux error with second- and fourth-order accurate finite-difference equations. II. Application to systems comprising first-order chemical reactions. *J. Comput. Chem.* **2005**, *26*, 633−641. (l) Rudolph, M. Attaining exponential convergence for the flux error with second- and fourth-order accurate finite-difference equations. Part 3. Application to electrochemical systems comprising second-order chemical reactions. *J. Comput. Chem.* **2005**, *26*, 1193−1204.

(22) (a) Arrigoni, F.; Rizza, F.; Vertemara, J.; Breglia, R.; Greco, C.; Bertini, L.; Zampella, G.; De Gioia, L. Rational Design of Fe₂(μ-PR₂)₂(L)₆ Coordination Compounds Featuring Tailored Potential Inversion. *ChemPhysChem* **2020**, *21*, 2279−2292. (b) Gross, M.; Jordan, J. Voltammetry at glassy carbon electrodes. *Pure Appl. Chem.* **1984**, *56*, 1095−1129. (c) Guidelli, R.; Compton, R. G.; Feliu, J. M.; Gileadi, E.; Lipkowski, J.; Schmickler, W.; Trasatti, S. Definition of the transfer coefficient in electrochemistry (IUPAC Recommendations 2014). *Pure Appl. Chem.* **2014**, *86*, 259−262. (d) Guidelli, R.; Compton, R. G.; Feliu, J. M.; Gileadi, E.; Lipkowski, J.; Schmickler, W.; Trasatti, S. Defining the transfer coefficient in electrochemistry: An assessment (IUPAC Technical Report). *Pure Appl. Chem.* **2014**, *86*, 245−258.

(23) Bieniasz, L. K.; Speiser, B. Use of sensitivity analysis methods in the modelling of electrochemical transients: Part 3. Statistical error/uncertainty propagation in simulation and in nonlinear least-squares parameter estimation. *J. Electroanal. Chem.* **1998**, *458*, 209−229.

(24) (a) Wu, T.-J.; Chen, C.-S.; Yeh, W.-Y.; Kuo, T.-S.; Lee, G.-H. Communication of metal ions in the dinuclear ruthenium complexes containing 4,4′-bipyridine, 1,4-diisocyanobenzene, and pyrazine bridging ligands: Synthesis, characterization and structure determination. *Inorg. Chim. Acta* **2010**, *363*, 2553−2560. (b) Huang, J.; Lin, R.; Wu, L.; Zhao, Q.; Zhu, C.; Wen, T. B.; Xia, H. Synthesis, Characterization, and Electrochemical Properties of Bisosmabenzenes Bridged by Diisocyanides. *Organometallics* **2010**, *29*, 2916−2925.

(25) (a) Gong, Z.-L.; Zhong, Y.-W.; Yao, J. Conformation-Determined Through-Bond versus Through-Space Electronic Communication in Mixed-Valence Systems with a Cross-Conjugated Urea Bridge. *Chem. - Eur. J.* **2015**, *21*, 1554−1566. (b) Barrière, F.; Geiger, W. E. Use of Weakly Coordinating Anions to Develop an Integrated Approach to the Tuning of ΔE₁/₂ Values by Medium Effects. *J. Am. Chem. Soc.* **2006**, *128*, 3980−3989. (c) Hildebrandt, A.; Miesel, D.; Lang, H. Electrostatic interactions within mixed-valent compounds. *Coord. Chem. Rev.* **2018**, *371*, 56−66. (d) D'Alessandro, D. M.; Keene, F. R. A cautionary warning on the use of electrochemical measurements to calculate comproportionation constants for mixed-valence compounds. *Dalton Trans* **2004**, 3950−3954. (e) Vilà, N.; Zhong, Y.-W.; Henderson, J. C.; Abruña, H. D. Anthracene-Bridged Binuclear Ruthenium Complexes: Electrochemical and Spectroscopic Evidence of Electronic Communication Through the π System. *Inorg. Chem.* **2010**, *49*, 796−804.

(26) (a) Diallo, A. K.; Absalon, C.; Ruiz, J.; Astruc, D. Ferrocenyl-Terminated Redox Stars: Synthesis and Electrostatic Effects in Mixed-Valence Stabilization. *J. Am. Chem. Soc.* **2011**, *133*, 629−641. (b) Diallo, A. K.; Daran, J.-C.; Varret, F.; Ruiz, J.; Astruc, D. How Do Redox Groups Behave around a Rigid Molecular Platform? Hexa(ferrocenylethynyl)benzenes and Their "Electrostatic" Redox Chemistry. *Angew. Chem., Int. Ed.* **2009**, *48*, 3141−3145.

(27) Xie, Q.; Perez-Cordero, E.; Echegoyen, L. Electrochemical detection of C₆₀⁶⁻ and C₇₀⁶⁻: Enhanced stability of fullerides in solution. *J. Am. Chem. Soc.* **1992**, *114*, 3978−3980.

(28) Pickett, C. J. A simple hydrocarbon electrolyte: completing the electron-transfer series [Fe₄S₄(SPh)₄]¹⁻/²⁻/³⁻/⁴⁻. *J. Chem. Soc., Chem. Commun.* **1985**, 323−326.

(29) Bard, A. J.; Faulkner, L. R. *Electrochemical Methods: Fundamentals and Applications*, 2nd ed.; John Wiley & Sons, Inc.: Hoboken, NJ, 2001.

(30) (a) Li, Y.; Rauchfuss, T. B. Synthesis of Diiron(I) Dithiolato Carbonyl Complexes. *Chem. Rev.* **2016**, *116*, 7043−7077. (b) Smith, D. A.; Zhuang, B.; Newton, W. E.; McDonald, J. W.; Shultz, F. A. Two-electron transfer accompanied by metal-metal bond formation. Synthesis and electrochemistry of dinuclear molybdenum and tungsten carbonyl thiolates. *Inorg. Chem.* **1987**, *26*, 2524−2531. (c) Shyu, S. G.; Calligaris, M.; Nardin, G.; Wojcicki, A. Reactions leading to formation and cleavage of metal-metal and metal-μ-phosphido bonds in binuclear molybdenum and tungsten complexes. Structural analyses of W₂(CO)₈(μ-PPh₂)₂ and its two-electron reduction product, [Li(THF)₃]₂[W₂(CO)₈(μ-PPh₂)₂]. *J. Am. Chem. Soc.* **1987**, *109*, 3617−3625.

(31) Williams, D. B. G.; Lawton, M. Drying of Organic Solvents: Quantitative Evaluation of the Efficiency of Several Desiccants. *J. Org. Chem.* **2010**, *75*, 8351−8354.

(32) (a) Havlík, M.; Dolenský, B.; Kessler, J.; Císařová, I.; Král, V. A new synthetic strategy to prepare throne and calix diastereoisomers of parallel tris-Tröger's bases. *Supramol. Chem.* **2012**, *24*, 127−134. (b) Goldeman, W.; Nasulewicz-Goldeman, A. Synthesis and antiproliferative activity of aromatic and aliphatic bis-[aminomethylidene(bisphosphonic)] acids. *Bioorg. Med. Chem. Lett.* **2014**, *24*, 3475−3479.